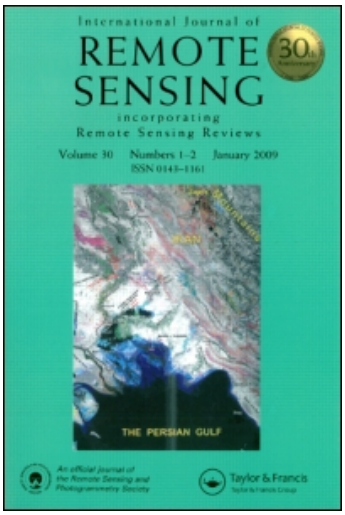

International Journal of Remote Sensing
Publication details, including instructions for authors and subscription information:
http://www.informaworld.com/smpp/title~content=t713722504

Prediction of forest canopy light interception using three-dimensional airborne LiDAR data

H. Lee [a]; K. C. Slatton [ab]; B. E. Roth [c]; W. P. Cropper [c]
[a] Department of Electrical and Computer Engineering, University of Florida, Gainesville, Florida 32611, USA [b] Department of Civil and Coastal Engineering, University of Florida, Gainesville, Florida 32611, USA [c] School of Forest Resources and Conservation, University of Florida, Gainesville, Florida 32611, USA

First Published:January2009

To cite this Article Lee, H., Slatton, K. C., Roth, B. E. and Cropper, W. P.(2009)'Prediction of forest canopy light interception using three-dimensional airborne LiDAR data',International Journal of Remote Sensing,30:1,189 — 207
To link to this Article: DOI: 10.1080/01431160802261171
URL: http://dx.doi.org/10.1080/01431160802261171

International Journal of Remote Sensing
Vol. 30, No. 1, 10 January 2009, 189–207

Taylor & Francis
Taylor & Francis Group

Prediction of forest canopy light interception using three-dimensional airborne LiDAR data

H. LEE†, K. C. SLATTON*†‡, B. E. ROTH§ and W. P. CROPPER JR§
†Department of Electrical and Computer Engineering, University of Florida, Gainesville, Florida 32611, USA
‡Department of Civil and Coastal Engineering, University of Florida, Gainesville, Florida 32611, USA
§School of Forest Resources and Conservation, University of Florida, Gainesville, Florida 32611, USA

(*Received 2 March 2007; in final form 17 August 2007*)

The amount of light intercepted by forest canopies plays a crucial role in forest primary production. However, the photosynthetically active part of this intercepted solar radiation (IPAR) is difficult to measure using traditional ground-based techniques. *In situ* measurement of IPAR requires labour-intensive field work, often resulting in limited datasets, especially when collected over extensive areas. Remote sensing methods have been applied to the estimation of light interception in forests, but until recently have been restricted to two-dimensional image data. These approaches do not directly account for the three-dimensional structure of forested canopies, and therefore predicting IPAR for arbitrary sun positions is problematic. We utilized a 3D point cloud dataset acquired via an airborne laser ranging (LiDAR) system to predict *in situ* measured IPAR. This was achieved by defining a field-of-view (scope) function between observer points just above the forest floor and the sun, which relate IPAR to the LiDAR data over southern pine experimental plots containing a wide range of standing biomass. A conical scope function with an angular divergence from the centreline of $\pm 7^{\circ}$ provided the best agreement with the *in situ* measurements. This scope function yielded remarkably consistent IPAR estimates for different pine species and growing conditions. IPAR for loblolly stands, which have diffuse canopy architecture, was slightly underestimated.

1. Introduction

Forest productivity is generally a function of leaf area index (LAI), as is well documented for southern pine forests (McCrady and Jokela 1998, Jokela and Martin 2000, Martin and Jokela 2004, Samuelson *et al.* 2004). Light attenuation through the canopy depends strongly on the amount of foliage in the stand (Gholz *et al.* 1991, MacFarlane *et al.* 2003), and therefore it is not surprising that net forest productivity has been positively and linearly related to the amount of photosynthetically active radiation (PAR) that is absorbed or intercepted by canopies (Monteith 1972, Dalla-Tea and Jokela 1991, McCrady and Jokela 1998). The quantity of PAR that is intercepted (IPAR) is largely determined by the amount of foliage in the canopy as well as its orientation (Colbert *et al.* 1990, McCrady and

*Corresponding author. Email: slatton@ece.ufl.edu

International Journal of Remote Sensing
ISSN 0143-1161 print/ISSN 1366-5901 online
http://www.tandf.co.uk/journals
DOI: 10.1080/01431160802261171

Jokela 1996, Landsberg and Gower 1997, Kucharik *et al.* 1998). However, the ability of trees to support leaf area and intercept light decreases with environmental stresses (Waring and Schlesinger 1985, Hebert and Jack 1998), such as soil nutrition and water limitations. The relationship between leaf area and light interception may also be modified by stand developmental processes (Martin and Jokela 2004). Leaf area and incident radiation have been successfully used to regionally model loblolly pine productivity across the south-east USA (Sampson and Allen 1999) and are the key drivers in process-based models of forest productivity (Wang and Jarvis 1990, Cropper and Gholz 1993, Battaglia and Sands 1998, MacFarlane *et al.* 2003). However, IPAR estimates across the landscape are limited by a lack of available radiation measurements, which are the most sparsely measured of routine climatologic data (Aber and Freuder 2000).

Traditional measurement of IPAR is time consuming, which is problematic given the changing light conditions throughout the day. The light incident on a particular forest canopy is constantly changing in both direction and intensity (Gay *et al.* 1971). As a result, the proportion of intercepted radiation may need to be corrected to a constant sun angle from zenith in order to facilitate repeated measurements through time (Will *et al.* 2005). Additionally, southern pine foliage exhibits strong seasonal dynamics and rapid responses to altered nutrition (Gholz *et al.* 1991), thus requiring frequent measurement of IPAR. As an alternative, remote sensing methods have been utilized to estimate canopy parameters, such as LAI, that are related to sunlight penetration through the canopy. However, since the sun constantly changes position and forest canopies exhibit strong three-dimensional structural variations, it is not sufficient to estimate PAR from traditional 2D data, such as multi-spectral imagery (Butson *et al.* 2002) or polarimetric synthetic aperture radar (Saatchi *et al.* 1994). Explicit 3D structural information is needed to predict sunlight transmission for different sun angles. While interferometric synthetic aperture radar (InSAR) can provide some 3D information, it is generally of insufficient spatial resolution to adequately measure stand-level variations (Slatton *et al.* 2001). Airborne light detection and ranging (LiDAR) systems on the other hand can provide both high spatial resolution and canopy penetration in a 3D point cloud format. For example, airborne LiDAR (also known as Airborne Laser Swath Mapping (ALSM)) measurements have been reliably related to *in situ* measurements of individual tree and stand structure (Holmgren *et al.* 2003, Lim *et al.* 2003, Maltamo *et al.* 2004, Farid *et al.* 2006), and has also been used to successfully estimate IPAR for maize and sunflower crops (Holdcroft *et al.* 2005). For this investigation, we show that it is possible to directly exploit the 3D nature of LiDAR data to estimate sunlight intercepted by the forest canopy while accounting for variations in sun angle.

There are two major classes of airborne laser ranging technologies currently in use: (1) large-footprint, full-waveform systems; and (2) small-footprint, discrete-return systems. Large-footprint LiDAR systems, such as the NASA Laser Vegetation Imaging Sensor (LVIS) (Drake *et al.* 2002) and Scanning LiDAR Imager of Canopies by Echo Recovery (SLICER) (Lefsky *et al.* 1999a), generally have footprint diameters on the order of tens of metres. The return signal is finely sampled over a long range gate, yielding a digitized reflected laser waveform. Because the large footprint spreads the transmitted photons over a wide area, many photons penetrate deep into the canopy, providing a densely sampled vertical profile. While large-footprint systems have been used to estimate forest biophysical parameters (Lefsky *et al.* 1999a, Lefsky *et al.* 1999b, Means *et al.* 1999, Ni-Meister

et al. 2001, Parker *et al.* 2001, Hyde *et al.* 2005), they are incapable of sensing structure over metre-scale spatial (horizontal) extent since the received waveform represents an integrated response for the entire area illuminated by the footprint. This limitation also leads to non-unique functional mappings from the waveforms back to forest structure because an infinite number of structural configurations can result in the same waveform shape. Also, full-waveform LiDAR sensors primarily remain research tools due to the excessive data volumes and associated per unit area acquisition costs (Flood 2002). The experimental NASA system, Experimental Advanced Airborne Research LiDAR (EAARL), combines waveform digitization with small-footprints (Brock *et al.* 2002). However, the laser pulse rate is comparatively low, which further reduces terrain sampling rates. The LiDAR data used in this work belongs to the small-footprint class of airborne laser-ranging technologies, which is more accessible to the wider geomorphologic and forestry communities.

Most studies employing small-footprint LiDAR data have to date focused on ground surface mapping. In those analyses, segmentation algorithms are usually applied to estimate the bare surface elevations by 'filtering out' returns from the vegetation using empirical thresholds on height variance or spatial connectedness of points (Weed *et al.* 2002, Haugerud *et al.* 2003, Zhang *et al.* 2003). The resulting set of non-ground LiDAR points can then be gridded to form a 2D image that is related to forest parameters, such as crown area (Farid *et al.* 2006). However, collapsing the 3D point data into a height image early in the processing can lead to a significant loss of information when attempting to characterize land cover with structural variations in all three spatial dimensions.

A few investigators have begun to analyse the 3D measurements of forest structure from small-footprint LiDAR (Eggleston *et al.* 2000, Todd *et al.* 2003). Todd *et al.* (2003) attempted to estimate indicator probabilities for different 'surfaces' representing different vertical strata in the canopy, such as overstorey, middle canopy, and lower canopy. Their approach involved interpolation of point data into surfaces and the *a priori* assumption of a preferred geometric shape for local distributions of points in canopies. They used a small-footprint LiDAR operating at an altitude of 750 m above ground, with a laser pulse rate of 20 kHz and a scan angle range of $\pm 15^{\circ}$, which produced 400-m wide swaths with a stated density of 8662 laser pulses per hectare (0.87 pulses per square metre). In this work we use a LiDAR density of roughly 1.83 transmitted pulses per square metre to better resolve the 3D canopy structure and thus avoid interpolating the data into surfaces.

The overall objective of this paper is to demonstrate a simple procedure for the estimation of IPAR in loblolly and slash pine plantations using airborne LiDAR remote sensing measurements. Specifically, we determined that a single parametric 'field of view' (scope) function can be found that enables reasonable estimates of IPAR across the set of widely varying canopy conditions studied in this trial. In addition to using discrete-return, small-footprint LiDAR measurements to ensure the results are broadly applicable to the forestry community, we use a relatively high laser pulse density and both first and last returns to achieve good 3D resolution and to examine what will be possible for other investigations as ALSM technology improves, yielding ever higher laser pulse rates. In §2, we describe the study area, how the ground truth IPAR measurements are collected, and our methodology for defining the scope functions. In §3 and §4, we present results and discussion. Finally, concluding remarks are made in §5.

2. Materials and methods

2.1 *Study site*

This investigation was carried out on a subset of plots at the Intensive Management Practices Assessment Center (IMPAC), located near Gainesville, Florida (29°45′N, 82°17′W) (figure 1(*a*)). A complete description of the study site and treatment history can be found in Swindel *et al.* (1988) (see also Jokela and Martin 2000). The forests native to this region are classified as subtropical moist forests. The topography in North Central Florida is generally very flat, with ground elevations in the study site varying as little as 2 m. The 24 plots in this study site were established in January 1983 as combinations of three binary states, such that three plots of each combination are present: [1] species (loblolly pine (*Pinus taeda* L.) vs. slash pine (*P. elliottii* Engelm. var. *elliottii*)); [2] understorey vegetation control (none vs. complete and sustained); and [3] fertilization (none vs. annual with macro- and micronutrients). In order to isolate PAR intercepted by the trees, we only considered plots where the understorey vegetation was controlled. A total of 12 plots were sampled consisting of three replicates for each of the species by fertilization treatment combinations (figures 1(*b*) and (*c*)). Each measurement plot was 0.027 ha

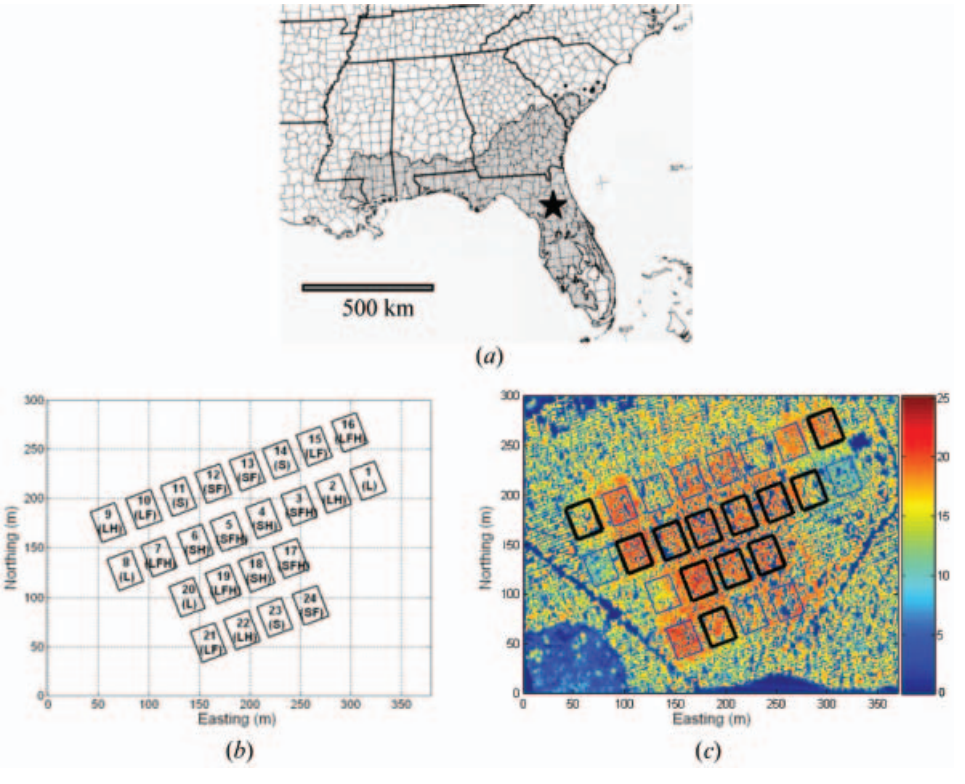

Figure 1. (*a*) The location of the IMPAC site with the geographic range of slash pine shaded and (*b*) the spatial arrangement of the 24 plots in the IMPAC study (plot codes: L=loblolly, S=slash, H=complete understorey vegetation control and F=fertilized). (*c*) Colour-coded elevation (above local ground) image derived from ALSM data (all units in metres). The 12 plots outlined in bold correspond to those used in this study (plots 2, 3, 4, 5, 6, 7, 9, 16, 17, 18, 19 and 22).

in size consisting of 40 planting positions on a 3.66 m × 1.83 m spacing arranged in five rows (beds) of eight trees each (figure 2). A summary of tree survival and solar angles at the time of measurement for each plot is provided in table 1. Over all 12 plots, the trees averaged 19 m tall with a live crown length of approximately 6 m (table 2). Sun position was defined in terms of two angles, θ (the angle from the easterly direction to the nadir projection of the observer-sun vector in the horizontal plane) and ϕ (the elevation angle of the sun above the horizon along the zenith), relative to the observation point at the origin of a translating (local) spherical coordinate frame (figure 3).

2.2 *Estimation of* in situ *IPAR*

Multiple techniques have been used to estimate the amount of PAR intercepted by forest canopies. The most common method is to estimate PAR incident at the top of the canopy and relate it to PAR incident below the canopy under uniform conditions (clear-sky or overcast) centred on solar zenith (Messier and Puttonen 1995). Many types of sensors have been employed to quantify the light environment under forest canopies, such as radiometers, photosensitive paper or chemicals, hemispherical canopy photographs, plant canopy analysers, or visual estimators of canopy density (Lieffers *et al.* 1999). For the results reported here, *in situ* measurements of IPAR were made using a combination of a LiCor LI-190 Quantum PAR sensor (LI-COR, Inc., Lincoln, NE) and an integrating PAR ceptometer (AccuPAR Linear Par Ceptometer, Model PAR-80, Pullman, WA). The AccuPAR is a battery-operated linear PAR ceptometer containing 80 independent

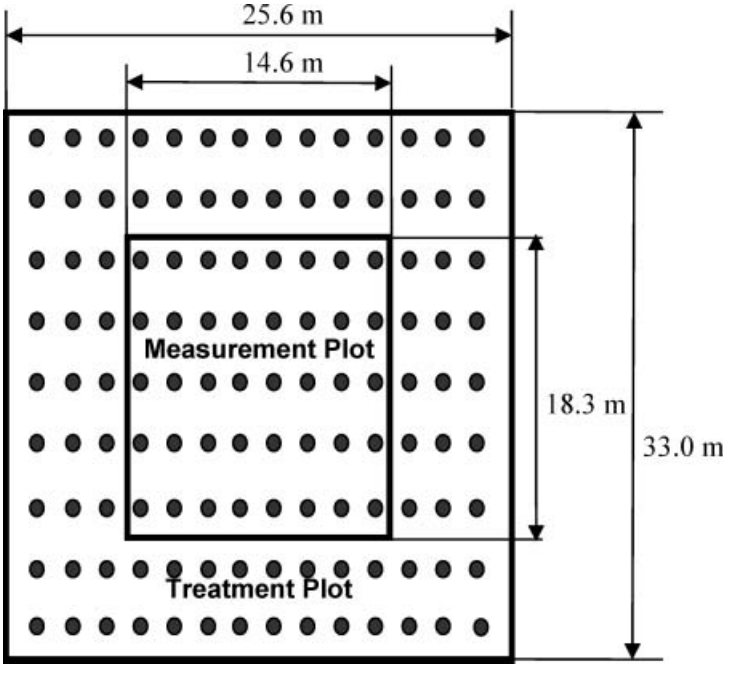

Figure 2. Schematic layout of a single plot. The interior measurement plot is shaded in grey, and is surrounded by the gross treatment plot. Each interior measurement plot was 0.027 ha in size and consisted of 40 planting positions. Grey circles indicate the nominal tree planting locations.

Table 1. Plot level inventory data detailing tree survival and solar angles at the time of the *in situ* PAR measurements. Data were collected in October 2005. A total of 40 trees were planted on each measurement plot in 1983. See figure 3 for a visualization of sun angles, which are expressed in degrees.

Species	Fertilized	Plot	Survival (no. of trees)	Sun angles (ϕ, θ)
Loblolly	No	2	38	(45, 55)
		9	29	(49, 69)
		22	27	(51, 98)
	Yes	7	25	(49, 67)
		16	35	(41, 48)
		19	28	(51, 95)
Slash	No	4	29	(44, 53)
		6	30	(47, 63)
		18	29	(51, 92)
	Yes	3	19	(43, 51)
		5	27	(47, 61)
		17	18	(51, 88)

Table 2. February 2005 inventory data from across the study site describing general tree dimensions. The trees were 22 year old at the time of the investigation.

Variable	Mean	Maximum	Minimum
Diameter at breast height (DBH) (cm)	19.86	35.3	3.8
Height (m)	19.36	26.0	6.6
Height to base of live crown (m)	13.61	20.6	3.7

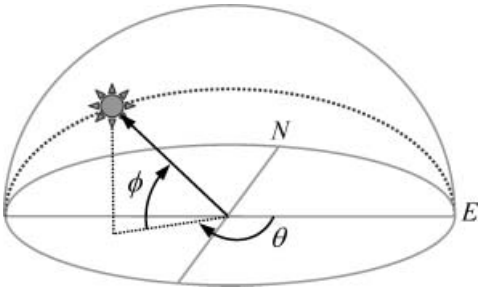

Figure 3. Solar angles (θ,ϕ) defined relative to an observer point at the origin of a local spherical coordinate frame. The elevation angle of the sun above the horizon along the zenith is defined as ϕ, while the angle from the easterly direction to the nadir projection of the observer-sun vector in the horizontal plane is defined as θ. All angles are reported in degrees. Local zenith is at (θ, 90°).

photodiodes, spaced 1 cm apart. The photodiodes measure PAR in the 400–700 nm spectral band in units of micromols per metre squared per second (μmol $m^{-2} s^{-1}$). The hemispherical field of view (FOV) was directed upward.

Above-canopy incident PAR (background), B_j, was collected using the LiCor LI-190 Quantum sensor which was placed in an open area adjacent to the study site. Concurrent below-canopy PAR samples, C_j, were collected over two measurement periods on 16 October 2005, using the integrating PAR ceptometer during a period of 2 hours centred about local solar zenith. At regular intervals during the sampling period side by side estimates were made in the open (background) to ensure

concurrence between the two sensors. Observations were taken during clear sky conditions to minimize contributions due to diffuse sky irradiance. The sun angle was noted during each *in situ* collection so that the corresponding sunlight penetration could be computed from the ALSM data. Ground measurements were collected from nine systematic transects spanning the width of each measurement plot (18.3 m) at a height of 1.5–2 m. Along each transect 16 light readings were taken and averaged to generate a single *in situ* data point per plot for each of two measurement periods. *In situ* IPAR, $I_{\text{in situ}}$, was computed using equation (1) with the average IPAR per plot computed from the average of the two readings ($J=2$)

$$I_{\text{in situ}} = \frac{1}{J}\left[\sum_{j=1}^{J}\left(1-\frac{C_j}{B_j}\right)\right], \tag{1}$$

where $I_{\text{in situ}} \in [0,1]$ since the intercepted sunlight flux is non-negative and the below-canopy value does not exceed the open sky value.

2.3 *Collection of ALSM data*

When flying at relatively low altitudes (e.g. 500–1000 m) and speeds near 50–70 m s^{-1}, most currently available ALSM systems with laser pulse rates of at least 25–50 kHz can provide sampling densities of one laser shot per square metre at ground level. For this work, we used data acquired on 11 October 2005 using the University of Florida's small footprint ALSM system (an Optech 1233 model), flown at 450 m above ground level (AGL) with a laser pulse rate of 33 kHz, scan rate of 30 Hz, and a scan angle range of $\pm 18^{\circ}$, resulting in a nominal laser shot density of 1.83 transmitted pulses per square metre on a single pass. We used both first and last returns from each shot to maximize sampling of the canopy and achieve roughly four times as many return samples per square metre (3.7 shots/m^2) as indicated in Todd *et al.* (2003). This configuration was used because we found that LiDAR sample densities on the order of a few per square metre were required to reliably resolve the 3D distribution of forest canopy for accurate estimates of IPAR. This sub-metre sampling supports the direct representation of the canopy as a point cloud rather than as a set of interpolated surfaces.

The laser operates with a beam divergence of 0.25 milliradians, a transmitted pulse duration (τ) of 10 ns (3 m of path length), and a near-infrared wavelength (λ) of 1064 nm (Carter *et al.* 2001). The system records the ranges of the first and last return pulses using a constant fraction discriminator at the output of an avalanche photodiode detector to detect the full width at half maximum (FWHM) points on the returned laser waveform (Slatton *et al.* 2005). As with all discrete-return ALSM systems, the pulse length imposes a lower limit on the vertical resolution between return pulses. The approximate minimum vertical distance for which separable first and last returns were recorded, given the 10 ns pulse duration, was 2.5 m.

2.4 *Isolating the vegetative contribution to IPAR*

Spatial variations in the sunlight flux through forest canopies are, in general, governed by local topography, latitude (sun angle), meteorological conditions (e.g. cloudiness, water vapour), and the amount and distribution of occluding vegetation. In this work, we are interested in capturing the contributing effects of vegetation, so a low-relief test site was chosen with a wide range of standing biomass. In order to relate the distribution of vegetation to ALSM observations, we first separated laser

light interception by the ground surface from that of the non-ground objects. We employed an adaptive multi-scale filter for this purpose (Kampa and Slatton 2004). The filter employed an information-theoretic hierarchical data segmentation scheme. First, the imaged area was classified into heavily vegetated and minimally vegetated areas. Then, a Gaussian mixture model (GMM) was estimated from the vertical histogram of aggregated last return points. An asymmetric decision rule was then applied to the GMM to ensure that the probability of missing a ground return was less than the probability of erroneously admitting a non-ground return in the bare surface estimate. The purpose of this decision rule was to admit LiDAR returns from small-scale surface features, such as scarps and stream banks. While it was possible that some vegetation returns near the ground may have been included in the segmented ground points, the probability was minimized in this investigation since the data collection was limited to the areas where the understorey vegetation had been removed.

To further reduce the probability of misclassifying ground points as non-ground points (i.e. vegetation), all points less than 1 m above the estimated ground surface were removed from consideration by assuming that the total error (system error + surface estimation error) was less than or equal to 1 m. This 1 m buffer is reasonable since field validation revealed that the rms error in the estimated ground surface under the canopy was much less than 1 m near ALSM points. Since that error can be larger (still less than 1 m) in small data voids where dense crowns prevent ALSM points from reaching the ground, the ALSM IPAR estimates are computed for an observation height of 2 m to correspond to the *in situ* IPAR measurement height.

2.5 *Optical scope functions*

Incident sunlight flux between the sun and a hypothetical observer under the forest canopy was determined by defining an optical field of view (scope function) for the observer. The scope functions originated at the observer and extended through the canopy in the direction of the sun. We examined a combination of cylindrical and conical geometries consisting of four unique scope functions: (1) a simple cylinder of 40 m in length; (2) a simple cone; (3) a cone weighted by the distance between the ALSM point and the observer; and (4) a cone weighted by both the distance between the ALSM point and the observer and the angular divergence from the conical centreline (figure 4). Secondary to this, within each function, five unique sizes were defined: diameters of 2 m, 3 m, 4 m, 5 m and 6 m for the cylinder and $\pm 5^\circ$, $\pm 7^\circ$, $\pm 10^\circ$, $\pm 15^\circ$ and $\pm 20^\circ$ angular divergences α from centreline for each of the conical functions. The choice of cylinder length was dependent upon the dominant tree height and the sun angles represented in the study area at the time of the investigation. In order to minimize computations, the shortest length that included all ALSM laser points was chosen. Since the tree height in the study area was generally less than 30 m and the sun angle greater than 40°, a 40 m cylinder length was utilized.

The weightings for the conical functions took two forms. In the first case, the occluding effect of a LiDAR point was weighted only by the distance δ between that point and the observer. We required a function, W_δ, that decreased monotonically with δ. It was also desirable to have a function with compact support to enforce upper and lower limits on the occluding effect. Maximum occlusion ($W_\delta = 1$) occurs when the LiDAR reflector is located at the observer point ($\delta = 0$). Zero occlusion

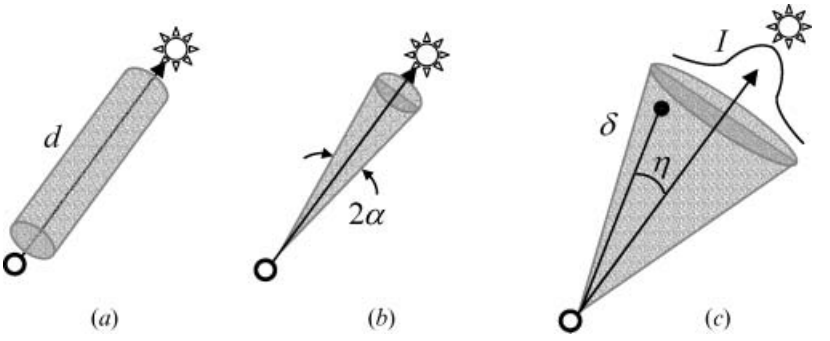

Figure 4. Different types of scope functions investigated. (*a*) Cylinder scope function with diameter *d*. (*b*) Cone scope function with angular divergence α. (*c*) A weighted cone scope function, where δ is the distance from an ALSM point in the scope to the observer, η is the angular deviation of that ALSM point from the centre line, and I is a truncated Gaussian irradiance distribution across the field of view.

(W_δ=0) occurs when the point in the scope is farther than $\delta_{\text{vanishing}}$ from the observer. The function must also be nonlinear to accommodate the optical property that an object's occluding effect becomes less sensitive to changes in its distance from the observer as that distance increases. A second order polynomial is the simplest such function that gives a 'graceful' decline in W_δ as δ approaches $\delta_{\text{vanishing}}$ by ensuring that derivatives up to 1st order remain continuous (see figure 5). The choice of $\delta_{\text{vanishing}}$=100 m is simply a conservative bound on the maximum expected path length from the observer to the canopy top given that canopies at the study site were all less than 30 m tall and that sun elevation angles of less than 20° are generally not of interest for IPAR studies.

In the second case, the occluding effect of an ALSM point relative to the observer was weighted by both its distance from the observer δ and its angular divergence η from the cone centreline. We followed similar reasoning for the η weighting as for the δ weighting. Namely, we wanted a function, W_η, that monotonically and continuously decreased from a maximum value at the scope centreline as a function of η to a minimum value at the cone's edge. This occluding effect should approach the cone edge in a smooth manner (continuous up to 1st order derivative), but it should not strictly reach zero at the cone edge since there can still be some occluding effect as long as the object is in the field of view. The function should be nonlinear to accommodate the optical property that an object's occluding effect becomes less sensitive to changes in its divergence angle as the divergence increases. A truncated Gaussian distribution was therefore used as a simple parameterization for the angular weighting of the sunlight intensity (relative irradiance). The Gaussian was preferred over a quadratic for W_η because it corresponded more closely to observations of direct solar irradiance versus angle (Halthore *et al.* 1996). The η weighting has the following characteristics, as depicted in figures 4 and 5: (a) the effective intensity of the sun's radiation I follows a Gaussian distribution from centreline up to $\pm 20°$; and (b) the minimum intensity is reached at 20° and maintains a constant value of 0.1 for larger angles. The η and δ weighting functions were applied to each ALSM point inside a given scope so that the maximum total weight was 1.0 and the minimum was 0. In our case, the minimum total weight never reached 0 since the maximum scope length $\delta_{\max}$ of 40 m was less than $\delta_{\text{vanishing}}$.

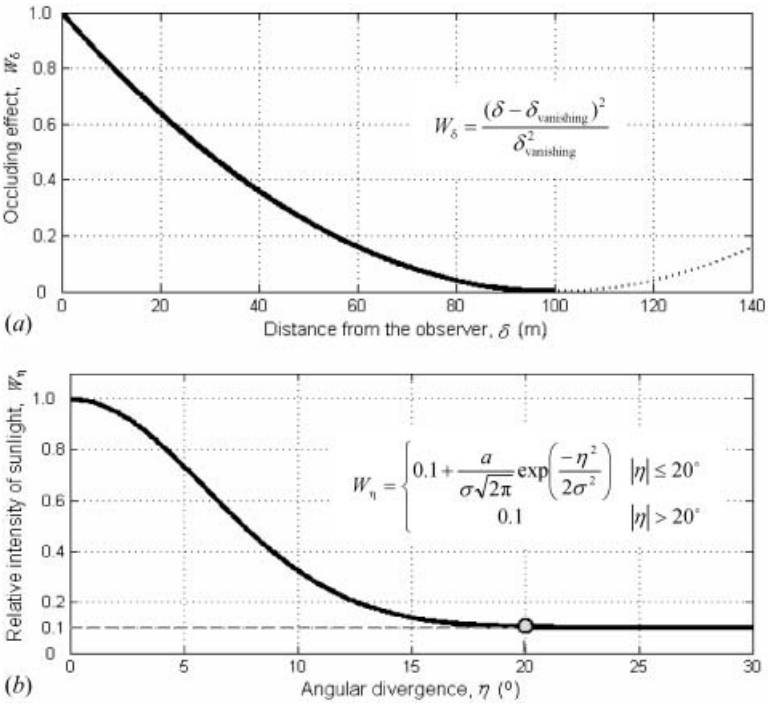

Figure 5. (*a*) The quadratic occluding effect weighting function W_δ with respect to distance from the observer. (*b*) The truncated Gaussian weighting function W_η with respect to angle from the line of sight, where $\sigma = 6^\circ$ and the scale factor $a = 13.5$.

2.6 *Estimation of IPAR from ALSM*

For each scope function, the point densities of non-ground laser returns inside the scope, originating 2 m above the ground surface, were computed. Since the type of scope function used was fixed for a given IPAR estimate over the study area, and therefore the volume of the scope was fixed, LiDAR point densities were computed simply by counting the number of non-ground laser returns inside the scope. Each scope function was given a constant orientation towards the position in the sky that the sun occupied during the corresponding *in situ* data collection. This procedure was iterated across each measurement plot in 1 m horizontal grid increments. The sun's angular position was computed for each ALSM estimate using the latitude and longitude of the study site in combination with the date and time of the ground truth measurement (Giesen 2005, Gronbeck 2005). This allowed for a direct comparison between *in situ* measured IPAR and ALSM estimated IPAR.

Since ALSM point clouds consist of irregularly spaced samples, with each location in the imaged area having variable point densities, the IPAR estimates derived from ALSM data, I_{ALSM}, were normalized by the local point density. The variation in point density in this study was small due to the fact that data from a single flight line was used. However, normalizing by point density would be crucial when working with LiDAR datasets composed of mosaics of multiple and partially overlapping flight lines. We utilized a simple normalized functional mapping

algorithm in order to estimate I_{ALSM} from the point density of LiDAR returns corresponding to the canopy at a specific observer point, denoted by i, in equation (2):

$$I_{\mathrm{ALSM}}(i) = \frac{\ln(\rho_{\mathrm{i}} + 1)}{\max\limits_{i \in 1,2,\ldots,M} \ln(\rho_{\mathrm{i}} + 1)}, \tag{2}$$

where ρ_{i} is the number of the ALSM non-ground points inside the scope at the ith location where each point's contribution has been weighted as described in §2.5, and M is the total number of I_{ALSM} calculations over the entire study site.

The number of ALSM points ρ in the scope function can in general vary from zero to some finite but large number L, which is not known a priori. I_{ALSM} was computed across the entire 370 m × 300 m study area in order to thoroughly sample the local foliage densities for normalization purposes (i.e. the denominator in equation (2)). The effective I_{ALSM} for each measurement plot was then computed as the average of all I_{ALSM}(i) within that measurement plot.

The simple nonlinear relationship in equation (2) was defined as a continuous-valued dimensionless measure bounded by 0 and 1, which could be used for comparisons with $I_{\mathrm{in\ situ}}$ in equation (1). While a linear scaling, such as $\rho/\max\rho$, could provide a linkage between $\rho \in [0,L]$ and $I_{\mathrm{ALSM}} \in [0,1]$, the logarithm provided the desired property that small differences in ρ would have significant impact on the calculation for ρ small but little impact for ρ large. Normalizing by the maximum value provides the unity upper bound. The arctangent could also have been used, which would have provided somewhat similar results. However, in that case the upper bound would have been fixed (no longer dependent on L) and therefore not related to the distribution of foliage in the study area in the same way that $I_{\mathrm{in\ situ}}$ was. The exact manner in which true IPAR increases as a function of foliage density is not generally known since it depends upon the particular arrangement and spectral absorbance of occluding objects, such as stems, branches and clumps of foliage. The goal of this investigation was to derive a set of simple scope functions with minimal parameterization and empirical calibration, such that they could be employed across a wide variety of forest types and conditions.

2.7 *Analysis*

I_{ALSM} was calculated across the 12 plots using all combinations of the four scope functions and five dimension classes, which resulted in 240 estimated values. The most appropriate overall scope function and dimension was selected by comparing the residuals between the estimated I_{ALSM} and the *in situ* measured IPAR for each plot. Analysis of variance (ANOVA) was performed on this dataset of residuals using SAS software (SAS Institute 2000). The best combination of scope function and dimension was selected using the LSMEANS option in the PROC GLM procedure. The PROC REG procedure was used in SAS in order to quantify the strength of the relationship between observed and estimated values of IPAR. We tested for the need for different equations for the main effects of species and fertilization using the one-way fixed group model. Differences among the treatments for *in situ* and ALSM derived IPAR were tested using ANOVA via the PROC GLM procedure in SAS. Separation of means analysis was done using the LSMEANS procedure in SAS.

3. Results

3.1 *Selection of the best scope function*

Analysis of variance indicated that there were large differences between scope functions in their ability to predict IPAR ($p<0.0001$). The performance was dependent on the physical dimensions as well as the shape of the scope functions. In figure 6, the average absolute error is plotted for each scope function. The smallest residuals for the cylindrical function occurred when a radius of 2.5 m was used. Based on the average absolute difference values, we found that the conical scope functions have the advantage of yielding smaller maximum errors (no greater than 0.17) than the cylindrical scope function (0.33) for a wide range of angles and weights. In the case of the conical scopes, we found the strongest dependence to be on the divergence angle α. An angle of $\alpha=7^\circ$ yielded the minimum mean squared error between I_{ALSM} and $I_{\mathrm{in\ situ}}$ regardless of weighting by distance δ and/or angle η. Thus, relatively narrow conical scope functions performed best overall, and within such scope functions, the position of individual ALSM points had a relatively weak effect on the IPAR estimate.

In terms of the sign of the error, we found that for the cylindrical functions, all radii less than 2.5 m resulted in underestimates of I_{ALSM} and radii greater than 2.5 m resulted in slight overestimates. For conical functions, small divergence angles ($\alpha\leqslant 5^\circ$) led to a slight underestimation of I_{ALSM}, while large divergence angles ($\alpha\geqslant 10^\circ$) led to an overestimation of I_{ALSM}. Although the underestimation of I_{ALSM} for small α and overestimation for large α were relatively small, the fact that those trends were consistent for all weighting schemes suggests that omitting indirect sky irradiance may have been the cause.

3.2 *Variation in IPAR*

Analysis of variance for both I_{ALSM} and $I_{\mathrm{in\ situ}}$ demonstrated a significant interaction between species and fertilization ($p=0.0276$ and $p=0.0957$ respectively) (table 3). Fertilized loblolly pine intercepted the most light, while non-fertilized loblolly intercepted the least (table 4). Fertilization did not have a statistically

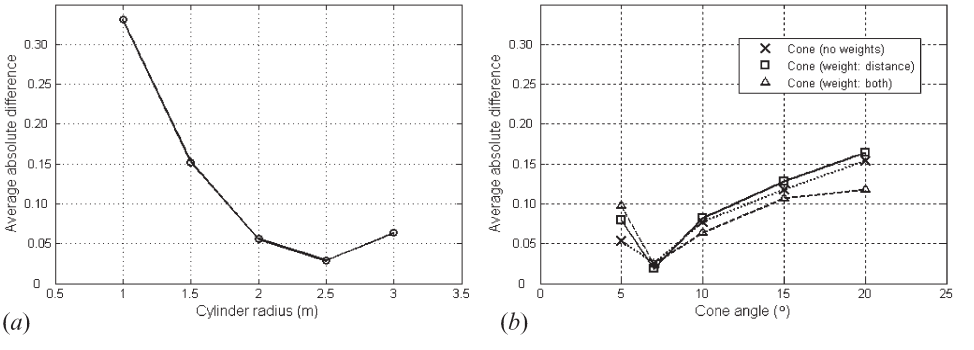

(*a*) (*b*)

Figure 6. Residual analysis comparing the two types of scope functions as dimensions change, where average absolute difference is simply the average absolute value of ALSM IPAR estimates minus *in situ* IPAR measurements. (*a*) Cylinder scope function performance with respect to diameter. (*b*) Performance of three different cone scope functions with respect to angular divergence. The conical scope function with an angle of 7° yielded the best overall estimates.

Table 3. Analysis of variance (ANOVA) table for *in situ* and estimated IPAR. *p*-values in bold are considered statistically significant at alpha (significance level) less than or equal to 0.1. Degrees of freedom are represented by df.

		In situ		ALSM estimate	
Source of variation	df*	MS†	*p*-value	MS	*p*-value
Species (S)	1	0.000108	0.8113	0.001800	0.3864
Fertilization (F)	1	0.002945	0.2334	0.003924	0.2132
S × F	1	0.012805	**0.0276**	0.007650	**0.0957**
Error	8	0.001772		0.002145	

* Degrees of freedom.
† Mean squared residual.

Table 4. Least squares estimates of IPAR measured *in situ* and estimated from ALSM. Using Bonferroni's least significant difference (LSD), differences between *in situ* and ALSM values in all four rows are not significant at alpha equal to 0.05. The cone function with $\alpha=7^\circ$ and weighted by distance is used in this analysis.

Species	Fertilized	*In situ*	ALSM
Loblolly	Yes	0.735	0.705
Slash	No	0.698	0.693
Slash	Yes	0.664	0.679
Loblolly	No	0.639	0.618

significant influence on light interception in the slash plots, although fertilized slash pine intercepted slightly less light than non-fertilized. We used the cone function with $\alpha=7^\circ$ and weighted by distance because (as can be seen in figure 6) that gave the minimum average absolute error.

3.3 *Residual analysis*

Overall the strength of the relationship between observed and predicted values of IPAR was strong; however, regression analysis determined that a bias in the prediction of remotely sensed estimates of IPAR existed between species. While there was no difference between the slopes of the equations between species ($p=0.4850$), there was a significant difference between intercepts ($p=0.0094$). Using the cone function with $\alpha=7^\circ$ and weighted by distance, IPAR for loblolly pine was slightly underestimated by the ALSM; however, slash pine was very close to the 1:1 line between observed and predicted (figure 7). The relatively small residuals are considered encouraging given the minimal parameterization of these scope functions.

4. Discussion

4.1 *Factors influencing* in situ *IPAR*

In general, fertilization builds leaf area and creates a denser canopy with high light interception (Sampson and Allen 1998). This was the case in this study where fertilized loblolly pine had the greatest levels of light interception. The lack of differences in light interception between fertilized and non-fertilized slash pine was

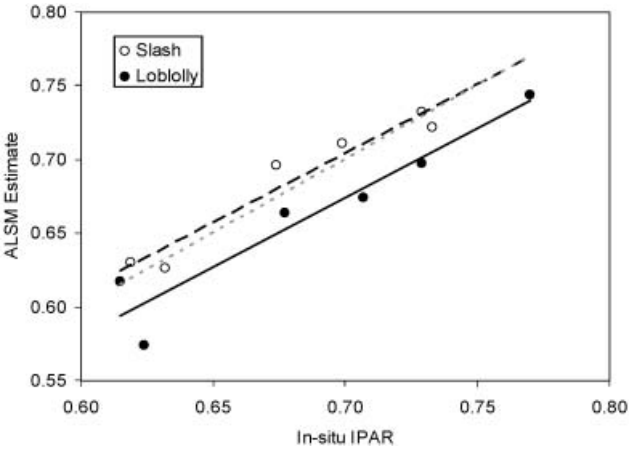

Figure 7. Relationship between observed (*in situ*) and estimated IPAR (from ALSM) using the cone function with $\alpha=7^\circ$ and weighted by distance. Separate equations were developed for each species since analysis indicated statistically different intercepts ($p=0.0094$). There was no significant difference for slopes between the equations so a common slope was used ($p=0.4850$). The light dotted line represents a hypothetical 1-to-1 ratio between observed and estimated. The equation for slash pine is $y=0.9351x+0.0493$ (dotted dark line), $r^2=0.935$, RMSE=0.0133; and for loblolly pine it is $y=0.944x+0.0132$ (solid line), $r^2=0.913$, RMSE=0.0197.

not unexpected since it is less responsive to fertilization than loblolly pine (Roth *et al.* 2007). Individual tree mortality resulted in open gaps in this study area and corresponding lower amounts of light interception in the fertilized slash pine treatment plots. However, this occurred only where mortality was the most recent, since with time the surrounding tree canopies expand to fill these gaps.

4.2 *Potential sources of error*

One potential source of unexplained error in this investigation may be the relatively low sun elevations at the time of *in situ* PAR data acquisition (between 41° and 51°). At these angles there was some contribution to PAR interception from trees in the surrounding gross treatment plot. While not quantified, it was assumed that tree attributes and mortality did not vary between the gross treatment and measurement portions of each plot.

Another potential source of error is the contribution of diffuse radiation. Laser light is phase-coherent and spectrally narrow-band, while sunlight is broad-band and incoherent. Therefore, in order to simplify the analysis, contributions from diffuse sky irradiance were neglected by virtue of using scope functions with narrow fields of view, collecting *in situ* measurements during clear sky conditions, and adjusting for the angle of the sun during the *in situ* measurements. For small α, too little interception was ascribed to the LiDAR points via equation (2), implying an overestimation of sunlight reaching the observer. This is likely caused by attributing too much of the measured light at the observer to direct solar irradiance because the contribution of indirect sky irradiance was neglected. A logical refinement of this work in future investigations would be to employ two separate scope functions to estimate IPAR, where one is tailored to capture the direct component of the total solar irradiance and the other tailored for the indirect component. However, a

rigorous examination of those two components would also require independent *in situ* measurements of each, which were not available for this investigation.

Varying proportions of standing woody material to leaves is another potential source of error. Neither the exact reflectance nor orientation was known for objects reflecting emitted laser light, such as leaves or branches. It was therefore not possible to derive an explicit closed form relationship between the laser light reflection and sunlight interception, since the laser beam interacted with an unknown mixture of reflectors inside each 15 cm diameter footprint.

4.3 *Bias between species*

The slight, yet consistent, underestimation of IPAR for loblolly pine was unexpected and is thought to be due to structural differences in their canopy architecture. Slash pine canopies are highly aggregated and clumped as opposed to loblolly pine, which is more diffused and continuous (Colbert *et al.* 1990). Since each laser return is the result of laser photons reflecting from occluding surfaces, the surfaces must be dense enough to reflect a measurable signal back to the ALSM receiver optics. In the case of the underestimate for loblolly pine, it is thought that the diffuse canopy allowed a greater number of laser photons to pass through for a given amount of foliage. Apparently, the clumped canopy properties of slash pine, which have made traditional measures of light interception difficult to model (Gholz *et al.* 1991), are in effect beneficial with respect to the ALSM methodology.

4.4 *Spatial variations of $IPAR_{ALSM}$*

The ability of ALSM to estimate the 3D spatial variations in IPAR with superior spatial resolution is illustrated in figure 8. The distribution of I_{ALSM} is computed using equation (2) assuming two different hypothetical sun angles at a 2 m elevation of scope origin. The conical scope function weighted by the distance between the ALSM point and the observer was used in this case. Due to the conical nature of the scope, less spatial aggregating of the IPAR estimates is expected by using observer heights farther off of the ground since a raised conical scope will have a smaller

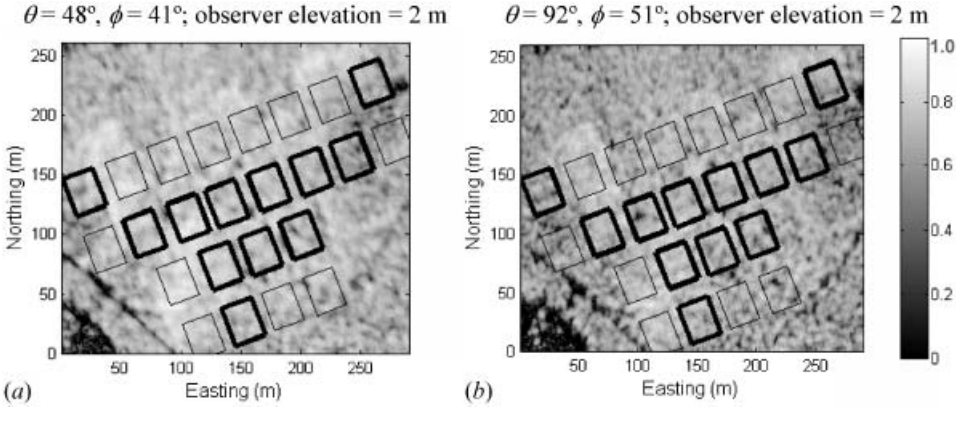

Figure 8. I_{ALSM} distribution for contrasting sun angles at an observer elevation of 2 m, illustrating the spatial resolution of I_{ALSM} computed in equation (2). The conical scope function weighted by the distance between the ALSM point and the observer was used in this case.

radius when it intersects the canopy points. Thus, raising the scope has the potential to reveal more detailed canopy structure.

5. Conclusions

We found that it is possible to define relatively simple parameterizations of light interception by forested canopies that allow for the prediction of IPAR from ALSM data. We employed simple optical scope functions that constrained the field-of-view from the ground through the canopy towards the sun in order to estimate IPAR from a 3D point cloud of ALSM data. Several scope functions were investigated, and a simple cone function with a divergence angle of $\pm 7^{\circ}$ and distance weighting was found to produce very good agreement with *in situ* IPAR measurements across species and treatment classes.

Although testing over different forest types was not possible due to a lack of additional ground truth data, we expect that our approach may perform well over other forests with minimal empirical calibration since we used scope functions described by a minimal set of parameters. In the case of the conical scope, we found the strongest dependence to be on a single parameter, the divergence angle α. This implies that the adjustment of one parameter may be sufficient to achieve reasonable agreement with ground-based measurement over differing forests. That performance would depend however on the nature of the understorey. ALSM data obtains fewer returns from the understorey than from the upper canopy. Thus, interception by the lower canopy and understorey may be understated using our approach. This limitation of the ALSM measurement could be mitigated however by limiting observer points to be higher than some specified elevation above the ground, as was done here. It should also be noted that if one were to use high observation elevations, the distance from the observer to the LiDAR points δ may then take on greater importance than it did in this study.

Estimates of IPAR using ALSM data and a calibrated scope function are likely to be more statistically reliable across wide areas than *in situ* estimates of IPAR derived from a limited sample population. This is because estimates of IPAR obtained from ALSM data are spatially dense due to the fact that the scope function can be translated in small spatial increments. Because ALSM provides us with metre-scale 3D structure rather than simply vertical structure, we can easily compute the number of laser returns, which corresponds to number of occlusions, from a hypothetical observer in the forest to any location in the sky. Furthermore, by knowing the site latitude and longitude and the sun's position on arbitrary dates and times, one could predict clear-sky IPAR for a variety of times of the year or times of the day using a couple of seasonally representative ALSM data sets (e.g. ALSM acquired during periods of peak and minimum leaf areas). Such predictions through time could be useful inputs for ecological process models.

Acknowledgements

This work was partially supported by the National Science Foundation (NSF) through the National Center for Airborne Laser Mapping (NCALM) under grant EAR-0518962. We are grateful for the assistance of the Forest Biology Research Cooperative (FBRC) in providing the *in situ* data. Special thanks to Rayonier, Inc., and to Drs Eric Jokela and Timothy Martin who provided access to the experimental study site. We also, thank Paul Proctor and Vanessa Tischler for technical assistance.

References

ABER, J.D. and FREUDER, R., 2000, Variation among solar radiation data sets for the Eastern US and its effects on predictions of forest production and water yield. *Climate Research*, **15**, pp. 33–43.

BATTAGLIA, M. and SANDS, P.J., 1998, Process-based forest productivity models and their application in forest management. *Forest Ecology and Management*, **102**, pp. 13–32.

BROCK, J.C., WRIGHT, C.W., SALLENGER, A.H., KRABILL, W.B. and SWIFT, R.N., 2002, Basis and methods of NASA Airborne Topographic Mapper LiDAR surveys for coastal studies. *Journal of Costal Research*, **18**, pp. 1–13.

BUTSON, C., FERNANDES, R., LATIFOVIC, R. and WENJUN, C., 2002, A robust approach for estimating LAI from Landsat TM/ETM+ imagery. *Proceedings of the IEEE International Geoscience Remote Sensing Symposium (IGARSS '02)*, **4**, pp. 2328–2330.

CARTER, W.E., SHRESTHA, R.L., TUELL, G., BLOOMQUIST, D. and SARTORI, M., 2001, Airborne Laser Swath Mapping Shines New Light on Earth's Topography. *EOS, Transactions American Geophysical Union*, **82**, pp. 549–555.

COLBERT, S.R., JOKELA, E.J. and NEARY, D.G., 1990, Effects of annual fertilization and sustained weed-control on dry-matter partitioning, leaf-area, and growth efficiency of juvenile loblolly and slash pine. *Forest Science*, **36**, pp. 995–1014.

CROPPER, W.P. and GHOLZ, H.L., 1993, Simulation of the carbon dynamics of a Florida slash pine plantation. *Ecological Modelling*, **66**, pp. 231–249.

DALLA-TEA, F. and JOKELA, E.J., 1991, Needlefall, canopy light interception, and productivity of young intensively managed slash and loblolly pine stands. *Forest Science*, **37**, pp. 1298–1313.

DRAKE, J.B., DUBAYAH, R.O., CLARK, D.B., KNOX, R.G., BLAIR, J.B., HOFTON, M.A., CHAZDON, R.L., WEISHAMPEL, J.F. and PRINCE, S., 2002, Estimation of tropical forest structural characteristics using large-footprint LiDAR. *Remote Sensing of Environment*, **79**, pp. 305–319.

EGGLESTON, N.T., WATSON, M., EVANS, D.L., MOORHEAD, R.J. and MCCOMBS, J.W., 2000, Visualization of airborne multiple-return LIDAR imagery from a forested landscape. *Proceedings of the ERIM International Conference on Geospatial Information in Agriculture Forestry*, **1**, pp. 470–477.

FARID, A., GOODRICH, D.C. and SOROOSHIAN, S., 2006, Using airborne Lidar to discern age classes of cottonwood trees. *Western Journal of Applied Forestry*, **21**, pp. 149–158.

FLOOD, M., 2002, From commercial data to commercial products: research priorities in the commercial sector. In *International Workshop on Three-dimensional Analysis of Forest Structure and Terrain Using LiDAR Technology*, Victoria, BC, March 2002, pp. 12–15.

GAY, L.W., KNOERR, K.R. and BRAATEN, M.O., 1971, Solar radiation variability on the floor of a pine plantation. *Agricultural Meteorology*, **8**, pp. 39–50.

GHOLZ, H.L., VOGEL, S.A., CROPPER, W.P., MCKELVEY, K., EWEL, K.C., TESKEY, R.O. and CURRAN, P.J., 1991, Dynamics of canopy structure and light interception in Pinus elliottii stands in North Florida. *Ecological Monographs*, **61**, pp. 35–51.

GIESEN, J., 2005, Sunshine Applet. Available online at: http://www.jgiesen.de/sunshine/ (accessed 21 October 2005).

GRONBECK, C., 2005, Sun Angle. Available online at: http://www.susdesign.com/sunangle/ (accessed 21 October 2005).

HALTHORE, R.N., SCHWARTZ, S.E., MICHALSKY, J.J., BERGIN, M.H., FERRARE, R.A., HOLBEN, B.N. and TEN BRINK, H.M., 1996, A closure experiment: prediction and measurement of direct-normal solar irradiance at the ARM Site. *American Geophysical Union Fall Meeting*, San Francisco, December, A11C-12, pp. 15–19.

HAUGERUD, R.A., HARDING, D.J., JOHNSON, S.Y., HARLESS, J.L., WEAVER, C.S. and SHERROD, B.L., 2003, High-Resolution LiDAR Topography of the Puget Lowland, Washington—A Bonanza for Earth Science. *GSA Today*, **13**, pp. 4–10.

HEBERT, M.T. and JACK, S.B., 1998, Leaf area index and site water balance of loblolly pine (*Pinus taeda* L.) across a precipitation gradient in east Texas. *Forest Ecology and Management*, **105**, pp. 273–282.

HOLDCROFT, C.J., CAMPBELL, C.L., DAVENPORT, I.J., GURNEY, R.J. and HOLDEN, N., 2005, Measurement of canopy geometry characteristics using LiDAR laser altimetry: A feasibility study. *IEEE Transactions on Geoscience and Remote Sensing*, **43**, pp. 2270–2282.

HOLMGREN, J., NILSSON, M. and OLSSON, H., 2003, Estimation of tree height and stem volume on plots using airborne laser scanning. *Forest Science*, **49**, pp. 419–428.

HYDE, P., DUBAYAH, R., PETERSON, B., BLAIR, J.B., HOFTON, M., HUNSAKER, C., KNOX, R. and WALKER, W., 2005, Mapping forest structure for wildlife habitat analysis using waveform lidar: Validation of montane ecosystems. *Remote Sensing of Environment*, **96**, pp. 427–437.

JOKELA, E.J. and MARTIN, T.A., 2000, Effects of ontogeny and soil nutrient supply on production, allocation, and leaf area efficiency in loblolly and slash pine stands. *Canadian Journal of Forest Research*, **30**, pp. 1511–1524.

KAMPA, K. and SLATTON, K.C., 2004, An adaptive multiscale filter for segmenting vegetation in ALSM data. *IEEE International Geoscience Remote Sensing Symposium (IGARSS)*, **6**, pp. 3837–3840.

KUCHARIK, C.J., NORMANA, J.M. and GOWER, S.T., 1998, Measurements of leaf orientation, light distribution and sunlit leaf area in a boreal aspen forest. *Agricultural and Forest Meteorology*, **91**, pp. 127–148.

LANDSBERG, J.J. and GOWER, S.T., 1997, *Applications of physiological ecology to forest management* (New York: Academic Press), p. 354.

LEFSKY, M.A., COHEN, W.B., ACKER, S.A., PARKER, G.G., SPIES, T.A. and HARDING, D., 1999a, LiDAR remote sensing of the canopy structure and biophysical properties of Douglas-fir western hemlock forests. *Remote Sensing of Environment*, **70**, pp. 339–361.

LEFSKY, M.A., HARDING, D., COHEN, W.B., PARKER, G. and SHUGART, H.H., 1999b, Surface LiDAR remote sensing of basal area and biomass in deciduous forests of eastern Maryland, USA. *Remote Sensing of Environment*, **67**, pp. 83–98.

LIEFFERS, V.J., MESSIER, C., STADT, K.J., GENDRON, F. and COMEAU, P.G., 1999, Predicting and managing light in the understory of boreal forests. *Canadian Journal of Forest Research*, **29**, pp. 796–811.

LIM, K., TREITZ, P., WULDER, M., ST-ONGE, B. and FLOOD, M., 2003, LiDAR remote sensing of forest structure. *Progress in Physical Geography*, **27**, pp. 88–106.

MACFARLANE, D.W., GREEN, E.J., BRUNNER, A. and AMATEIS, R.L., 2003, Modeling loblolly pine canopy dynamics for a light capture model. *Forest Ecology and Management*, **173**, pp. 145–168.

MALTAMO, M., MUSTONEN, K., HYYPPA, J., PITKANEN, J. and YU, X., 2004, The accuracy estimating individual tree variables with airborne laser scanning in a boreal nature reserve. *Canadian Journal of Forest Research*, **34**, pp. 1791–1801.

MARTIN, T.A. and JOKELA, E.J., 2004, Developmental patterns and nutrition impact radiation use efficiency components in southern pine stands. *Ecological Applications*, **14**, pp. 1839–1854.

MCCRADY, R.L. and JOKELA, E.J., 1996, Growth phenology and crown structure of selected loblolly pine families planted at two spacings. *Forest Science*, **42**, pp. 46–57.

MCCRADY, R.L. and JOKELA, E.J., 1998, Canopy dynamics, light interception, and radiation use efficiency of selected loblolly pine families. *Forest Science*, **44**, pp. 64–72.

MEANS, J.E., ACKER, S.A., HARDING, D.J., BLAIR, J.B., LEFSKY, M.A., COHEN, W.B., HARMON, M.E. and MCKEE, W.A., 1999, Use of large-footprint scanning airborne LiDAR to estimate forest stand characteristics in the western Cascades of Oregon. *Remote Sensing of Environment*, **67**, pp. 298–308.

MESSIER, C. and PUTTONEN, P., 1995, Spatial and temporal variation in the light environment of developing Scots pine stands: the basis for a quick and efficient method of characterizing light. *Canadian Journal of Forest Research*, **25**, pp. 343–354.

MONTIETH, J.L., 1972, Solar radiation and productivity in tropical ecosystems. *Journal of Applied Ecology*, **9**, pp. 747–766.

NI-MEISTER, W., JUPP, D.L.B. and DUBAYAH, R., 2001, Modeling LiDAR waveforms in heterogeneous and discrete canopies *IEEE Transaction on Geoscience and Remote Sensing*, **39**, pp. 1943–1958.

PARKER, G.G., LEFSKY, M.A. and HARDING, D.J., 2001, Light transmittance in forest canopies determined from airborne LiDAR altimetry and from in-canopy quantum measurements. *Remote Sensing of Environment*, **76**, pp. 298–309.

ROTH, B.E., JOKELA, E.J., MARTIN, T.A., HUBER, D.A. and WHITE, T.L., 2007, Genotype x environment interactions in selected loblolly and slash pine plantations in the southeastern United-States. *Forest Ecology and Management*, **238**, pp. 175–188.

SAATCHI, S.S., TREUHAFT, R. and DOBSON, M.C., 1994, Estimation of leaf area index over agricultural areas from polarimetric SAR images. *Proceedings of the IEEE International Geoscience Remote Sensing Symposium (IGARSS '94)*, **2**, pp. 826–828.

SAMPSON, D.A. and ALLEN, H.L., 1998, Light attenuation in a 14-year-old loblolly pine stand as influenced by fertilization and irrigation. *Trees*, **13**, pp. 80–87.

SAMPSON, D.A. and ALLEN, H.L., 1999, Regional influences of soil available water-holding capacity and climate, and leaf area index on simulated loblolly pine productivity. *Forest Ecology and Management*, **124**, pp. 1–12.

SAMUELSON, L.J., JOHNSEN, K. and STOKES, T., 2004, Production, allocation, and stemwood growth efficiency of *Pinus taeda* L. stands in response to 6 years of intensive management. *Forest Ecology and Management*, **192**, pp. 59–70.

SAS INSTITUTE, 2000, *SAS/STAT User's Guide: Version 8*, vols.1–3 (Cary, NC: SAS Institute).

SLATTON, K.C., CRAWFORD, M.M. and EVANS, B.L., 2001, Fusing interferometric radar and laser altimeter data to estimate surface topography and vegetation heights. *IEEE Transactions on Geoscience and Remote Sensing*, **39**, pp. 2470–2482.

SLATTON, K.C., CARTER, W. and SHRESTHA, R., 2005, A simulator for airborne laser swath mapping via photon counting. *Proceedings of SPIE 2005: Defense and Security Symposium*, **5794**, pp. 12–20.

SWINDEL, B.F., NEARY, D.G., COMERFORD, N.B., ROCKWOOD, D.L. and BLAKESLEE, G.M., 1988, Fertilization and competition control accelerate early southern pine growth on flatwoods. *Southern Journal of Applied Forestry*, **12**, pp. 116–121.

TODD, K., CSILLAG, F. and ATKINSON, P., 2003, Three-dimensional mapping of light transmittance and foliage distribution using LiDAR. *Canadian Journal of Remote Sensing*, **29**, pp. 544–555.

WANG, Y.P. and JARVIS, P.G., 1990, Description and validation of an array model—MAESTRO. *Agricultural and Forest Meteorology*, **51**, pp. 157–180.

WARING, R.H. and SCHLESINGER, W.H., 1985, *Forest ecosystems: concepts and management* (New York: Academic Press), p. 340.

WEED, C.A., CRAWFORD, M.M., NEUENSCHWANDER, A.L. and GUTIERREZ, R., 2002, Classification of LiDAR data using a lower envelope follower and gradient based operator. *Proceedings of the IEEE International Geoscience Remote Sensing Symposium (IGARSS '02)*, **3**, pp. 1384–1386.

WILL, R.E., NARAHARI, N.V., SHIVER, B.D. and TESKEY, R.O., 2005, Effects of planting density on canopy dynamics and stem growth for intensively managed loblolly pine stands. *Forest Ecology and Management*, **205**, pp. 29–41.

ZHANG, K., CHEN, S., WHITMAN, D., YAN, J. and ZHANG, C., 2003, A progressive morphological filter for removing nonground measurements from airborne LIDAR data. *IEEE Transaction on Geoscience and Remote Sensing*, **41**, pp. 872–882.